Supplementary Information for:

Diameter Dependent Performance of Silicon Nanowire Anodes Grown on 3D Current Collectors for Lithium-ion Batteries

Mei Li[a], Niraj Patel[a], Shalini Singh[a], David McNulty[a], Kevin M. Ryan*[a]*

[a] Department of Chemical Sciences and Bernal Institute, University of Limerick, Limerick V94 T9PX, Ireland

1. Experimental Section

Substrate Preparation: Stainless steel mesh (SSM, 304 grade, 400 mesh of 50 microns) was purchased from AliExpress, Co. Ltd. The 5.0 cm x 6.0 cm SSM was ultrasonically etched in 3.0 M hydrochloric acid (HCl), isopropyl alcohol (IPA) and deionized (DI) water, to remove the surface oxide layer and improve the contact between the current collector and the active material, followed by drying overnight at 70 °C in a vacuum oven. After that, different thicknesses of Sn (99.999%, Kurt J. Lesker) as catalysts were thermally evaporated onto these SSM pieces in a glove box-based evaporation system (Mbraun, MB-200B). The Sn thicknesses were varied from 10, 20, 50, to 100 nm on the SSM with the controlled average active material mass loading of ~ 0.11 mg/cm^2. The Sn-coated SSM substrates were dried overnight and stored in the Argon (Ar)-filled glove box before reactions to minimise oxidation.

Synthesis of Si Nanowires: Si NWs were grown on SSM current collectors using a previously published vapour-liquid-solid (VLS) growth system.[1,2] Reactions were carried out in a long-neck Pyrex 100 mL round-bottomed flask, the Sn-coated SSM substrate was placed around the bottom bulb area of the flask. The flask was then attached to a Schlenk line setup via a water

condenser and positioned vertically inside a three-zone vertical furnace. The temperature of the system was ramped up to 160 °C and a vacuum of ~ 200 mTorr was applied for 1 hour to remove any moisture from the system. Following this, the system was purged with Ar gas flow, and the flask was then ramped to reaction temperature under a constant Ar flow. A water condenser was used to control the reagent reflux and ensure that the reaction was kept under control. At a reaction temperature of 460 °C, a designed amount of mono-phenylsilane (PS, 97.0%, fluorochem) with Sn:Si molar ratio of 80 was injected into the system through a septum cap sealing the condenser, and the reaction was allowed to proceed for 30 min, different diameters of Si NWs were achieved via the vapour liquid solid growth mechanism. The furnace temperature program was switched off when the reaction finished and allowed to cool down naturally below 100 °C before opening the furnace and removing the Si NWs-coated SSM, followed by washing and sonication with toluene and IPA, drying overnight at 70 °C in the vacuum oven and storing under Ar before cell assembly. The synthetic method allowed for the direct preparation of electrodes as NWs are grown directly from the flexible current collector, with mass loadings of approximately 0.18 – 0.22 mg/cm^2 from the Si35, Si55, Si85 to Si100 used in this study. As a control experiment, pure Sn-100 seeds were also deposited on SSM, Si NWs with an average diameter of 40 nm (Figure S10) were directly grown on stainless-steel fibre cloth (SSFC) and stainless-steel sheet (SSS) with the same procedure, and then subjected to similar treatment for the following characterizations and electrochemical tests.

Materials Characterization: The respective mass of Si and Sn was determined through measurement using a Sartorius Ultra-Microbalance SE2 (repeatability ± 0.25 µg). The diameter distribution histogram was conducted by using Image J software and measuring more than 200 counts from the Scanning electron microscopy (SEM) images. SEM analysis was carried out using a Hitachi SU-70 system operating between 5 and 20 kV. The uncycled substrates required no prior treatment before SEM analysis. For transmission electron microscopy (TEM) analysis,

the NWs were removed from the growth substrate through sonication before being drop cast onto a lacy carbon TEM grid. TEM analysis was conducted at 200 kV on a JEOL JEM-2100F field emission microscope equipped with a Gatan Ultrascan CCD camera and EDAX Genesis EDS detector. For ex-situ analysis, the solid electrolyte interphase (SEI) layer was removed by soaking the electrodes in diethyl carbonate (DEC) before rinsing with 0.1 mM acetic acid, deionised water, and ethanol, separately, dry under Ar flow in the glovebox before imaging. X-ray diffraction (XRD) patterns were collected on a PANalytical Empyrean diffractometer equipped with a PIXcel3D detector and Cu Kα radiation source (λ = 1.5406 Å), operating at 40 kV and 40 mA at room temperature. X-ray photoelectron spectroscopy (XPS) was performed using a Kratos AXIS ULTRA spectrometer using monochromatic Al Kα 1486.58 eV. C 1s at 284.8 eV was used as the charge reference to determine the core level binding energies. The pass energy 160 eV was used for the survey spectra and 20 eV for the narrow regions. Raman spectroscopy measurements were performed using a Horiba Labraman 300 spectrometer system equipped with a 532 nm laser. Construction and peak fitting of synthetic peaks in narrow region spectra used a Shirley-type background and the synthetic peaks were of a mixed Gaussian-Lorenzian type for both XPS and Raman spectra. For post-mortem analysis of Raman spectra, the SEI layer was removed by the same treatment before TEM analysis.

Electrochemical Measurements: The electrochemical performance was evaluated using coin cells assembled in an Ar-filled glovebox. The cells consisted of the Sn-seeded Si NWs on an SSM current collector (Ø 10 mm) as the working electrode, glass fibre (Whatman™, GF/A) membrane as a separator, and lithium foil as the counter/reference electrode. 100 µl of 1.0 M $LiPF_6$ in ethylene carbonate/dimethyl carbonate (1:1 v/v) + 3.0 wt% vinylene carbonate (VC) was used as the electrolyte. The rate capability test (RCT) was analysed at 50, 100, 200, 500, and 1000 mA/g for 5 cycles, respectively, followed by the Galvanostatic measurements using

a Neware battery testing system in a potential range of 0.01 – 1.0 V (vs Li/Li^+) at 100 mA/g current density. The Cyclic Voltammetry (CV) tests were performed via a BioLogic MPG-2 multichannel potentiation over a 0.01 – 1.0 V (vs Li/Li^+) at a scan rate of 0.1 mV/s. The entire electrochemically active mass was used to calculate the currents applied.

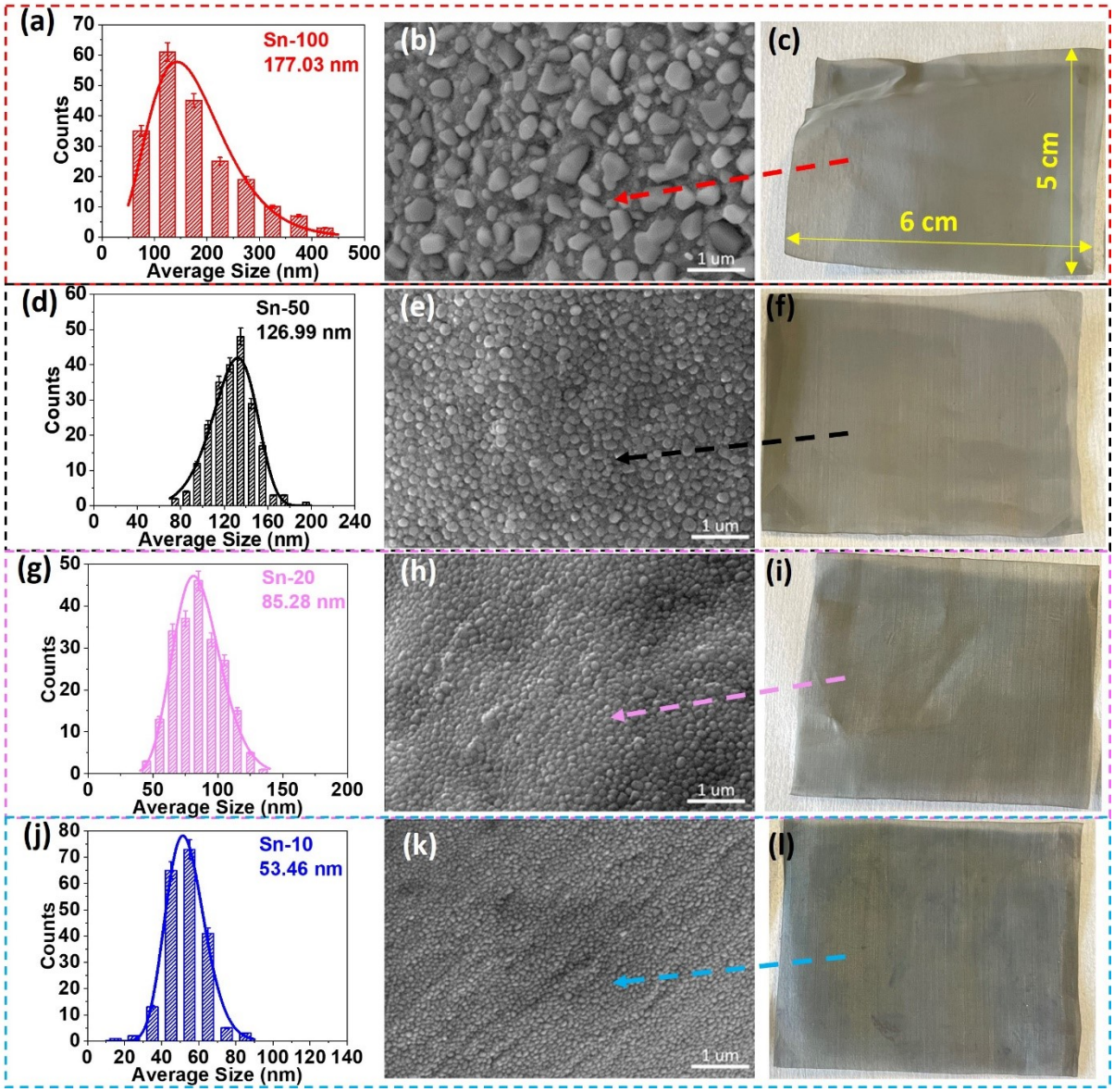

Fig. S1 The size histograms, SEM images and optical pictures of (a-c) Sn-100, (d-f) Sn-50, (g-i) Sn-20, and (j-l) Sn-10.

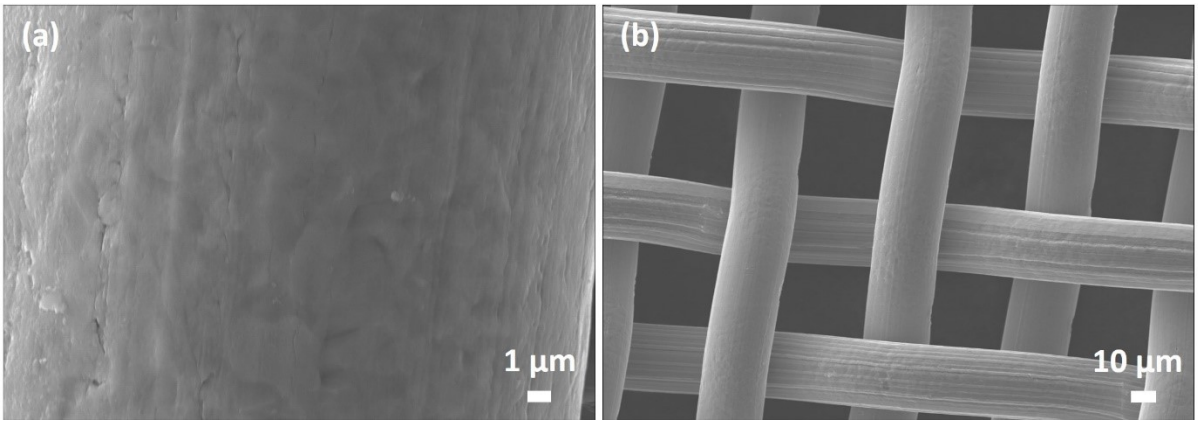

Fig. S2 (a) High and (b) low magnification SEM images of bare SSM substrate after etching.

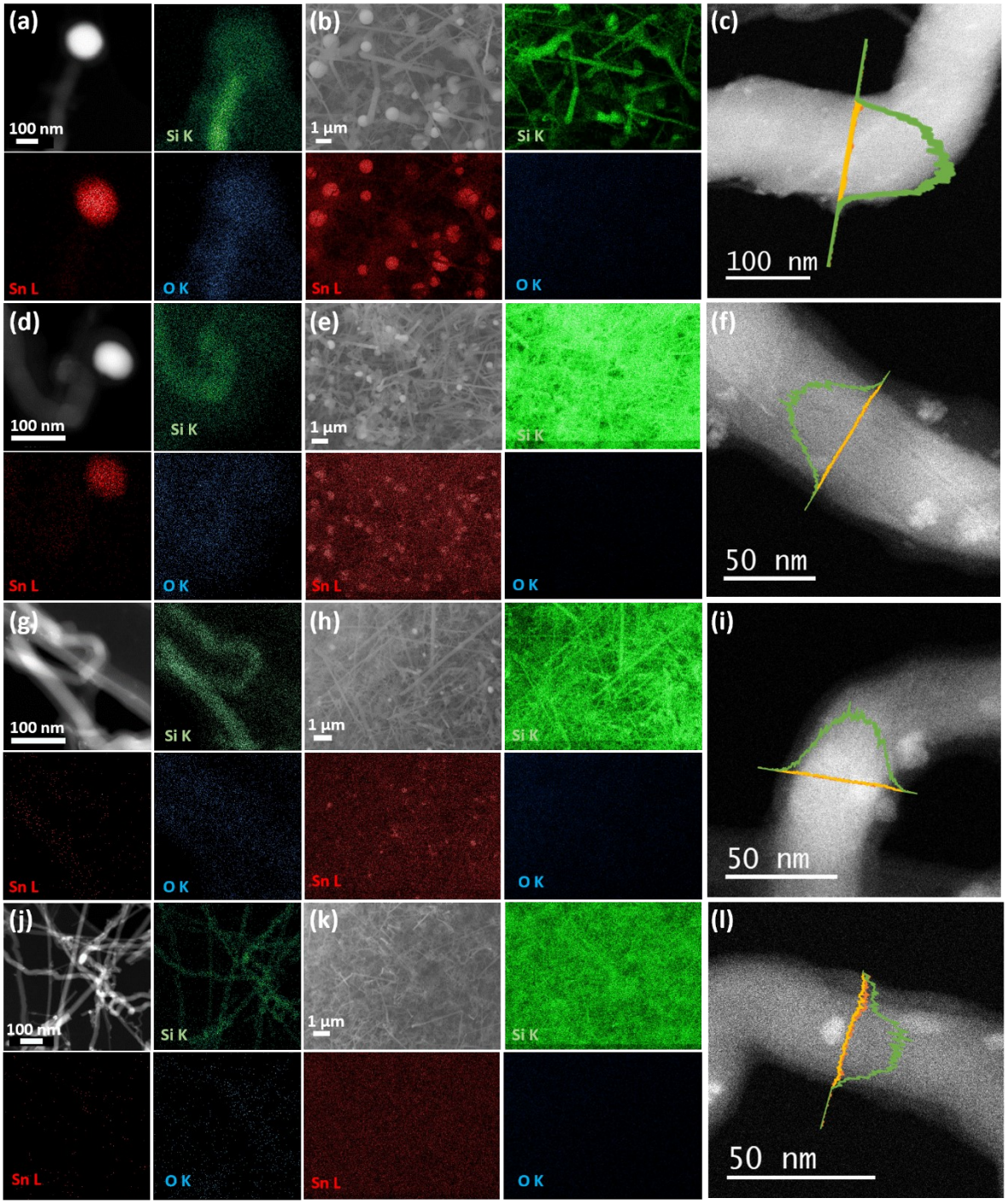

Fig. S3 The STEM, EDX element mapping, and line scan profiles of (a-c) Si100, (d-f) Si85, (g-i) Si55, (j-l) Si35. Colours codes for the STEM and EDX are green (Si), red (Sn), and blue (O), for line scan spectra are green (Si), orange (C), and yellow (O).

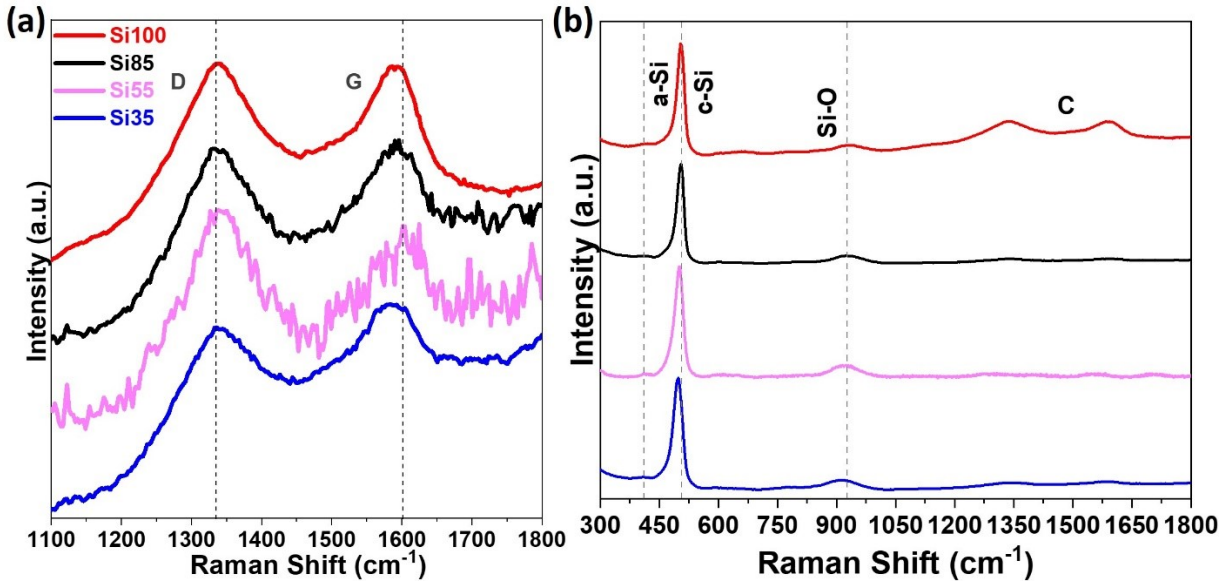

Fig. S4 Raman spectra of (a) the D and G bands deconvoluted from C, and (b) full range 300 – 1800 cm^{-1} from all samples (red) Si100, (black) Si85, (pink) Si55, and (blue) Si35.

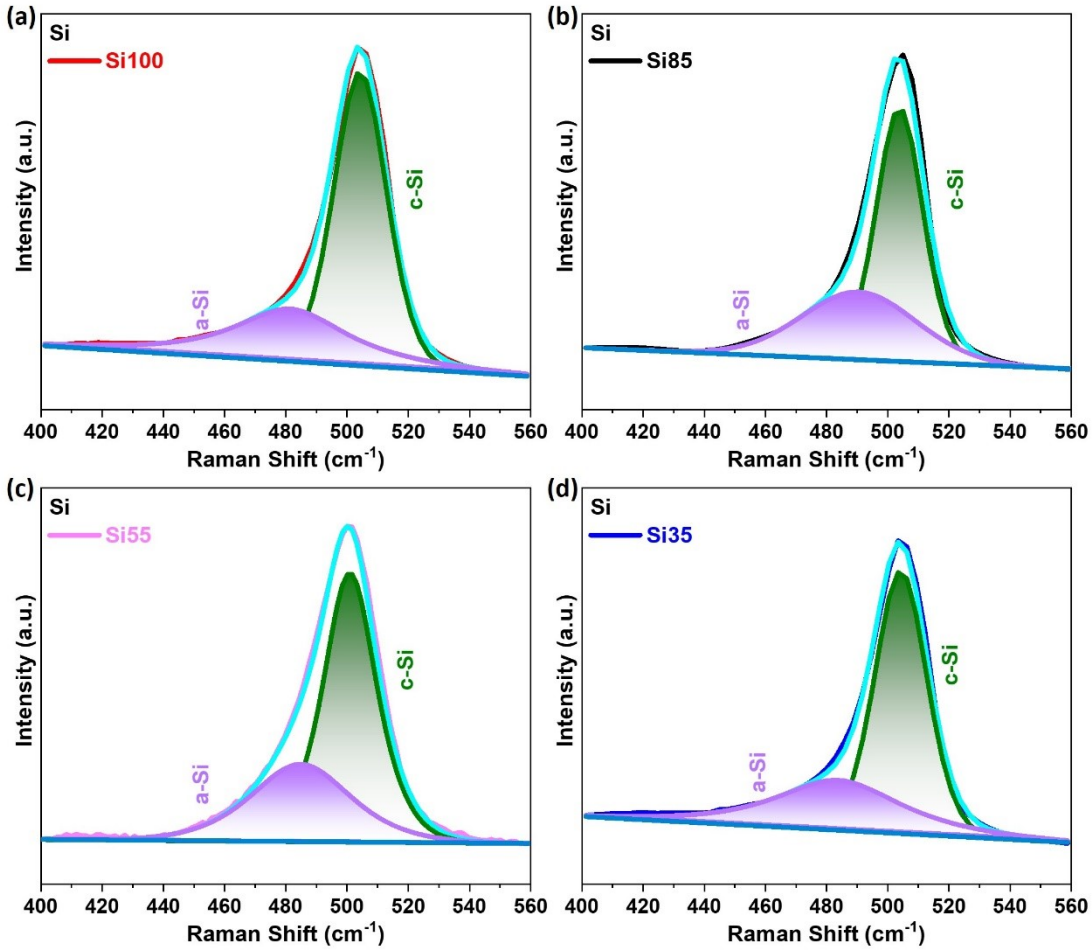

Fig. S5 Raman spectra deconvoluted peaks of amorphous Si (purple) and crystalline Si (green) for (a) Si100, (b) Si85, (c) Si55, and (d) Si35.

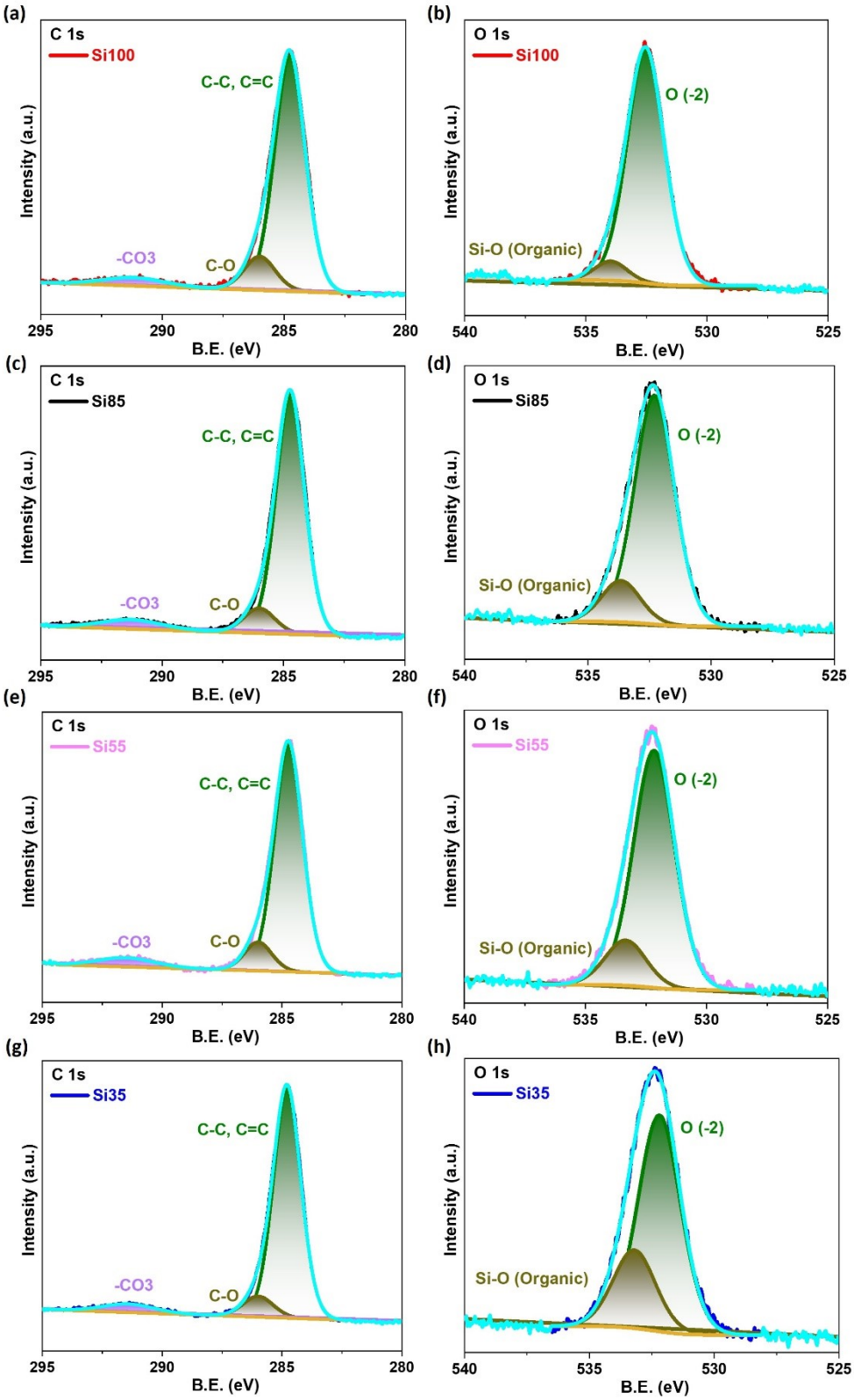

Fig. S6 High-resolution XPS C 1s and O 1s spectra for (a-b) Si100, (c-d) Si85, (e-f) Si55, and (g-h) Si35.

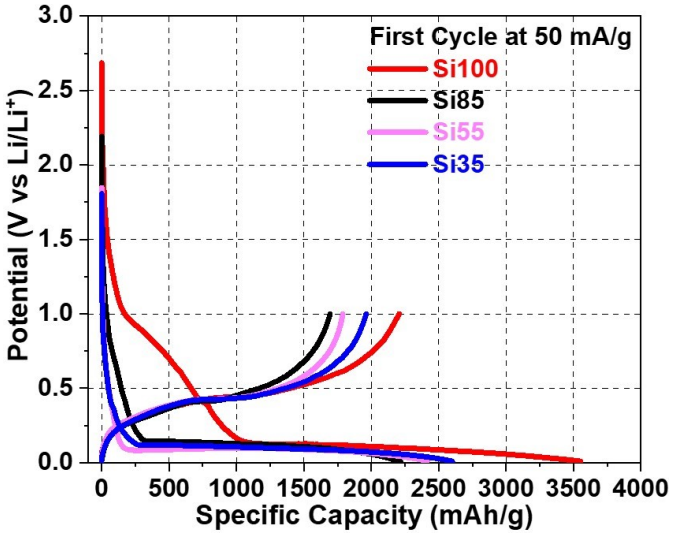

Fig. S7 The first cycle voltage–capacity profiles of (red) Si100, (black) Si85, (pink)Si55, and (blue) Si35 samples at an applied specific current of 50 mA/g in a full-scale voltage window of 0 to 3.0 V.

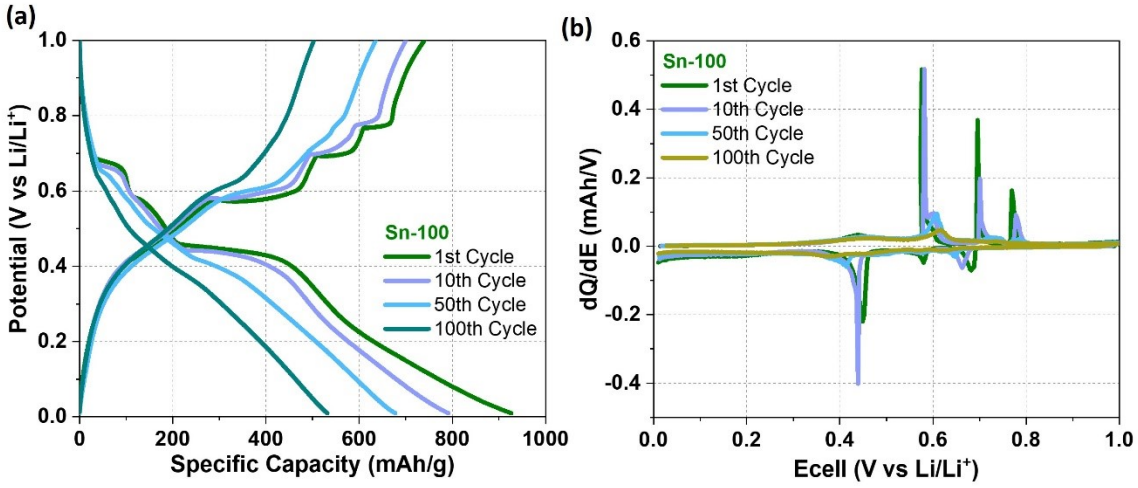

Fig. S8 (a) Voltage profile and (b) differential charge plot of Sn-100 electrode.

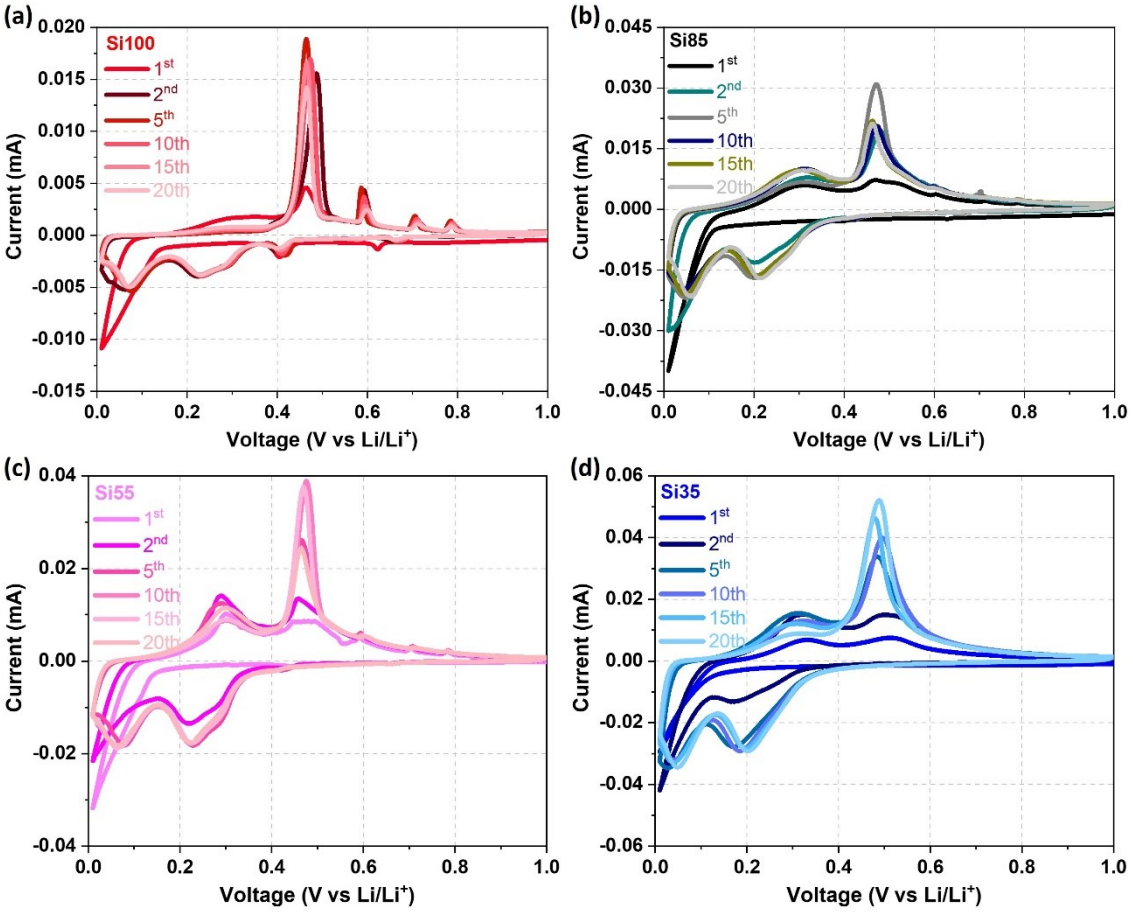

Fig. S9 Cyclic Voltammetry plots of (a) Si100, (b) Si85, (c) Si55, and (d) Si35 for 20 cycles at 0.1 mV/s from 0.01 – 1.0 V.

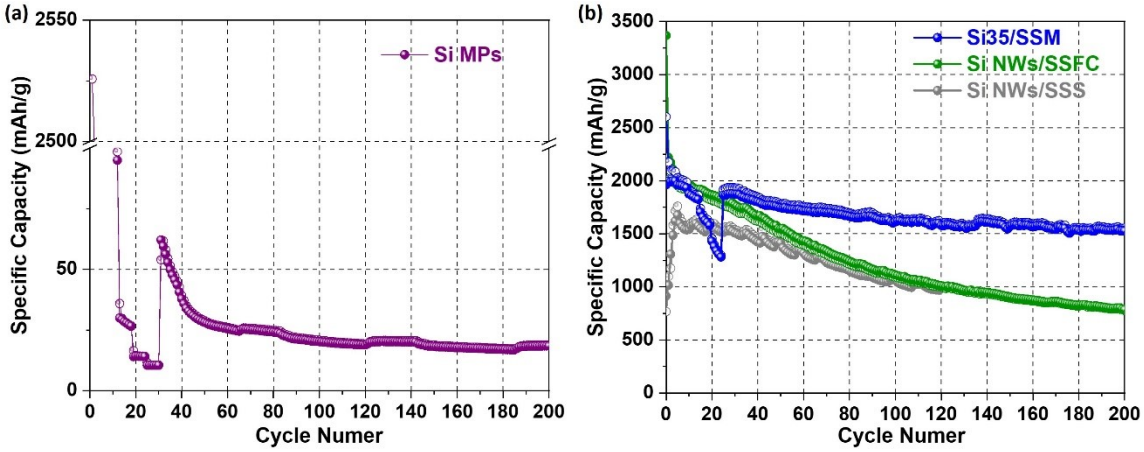

Fig. S10 Galvanostatic cycling profiles of (a) Si MPs, (b) comparison between Si35/SSM, Si NWs/SSFC, and Si NWs/SSS for 200 cycles.

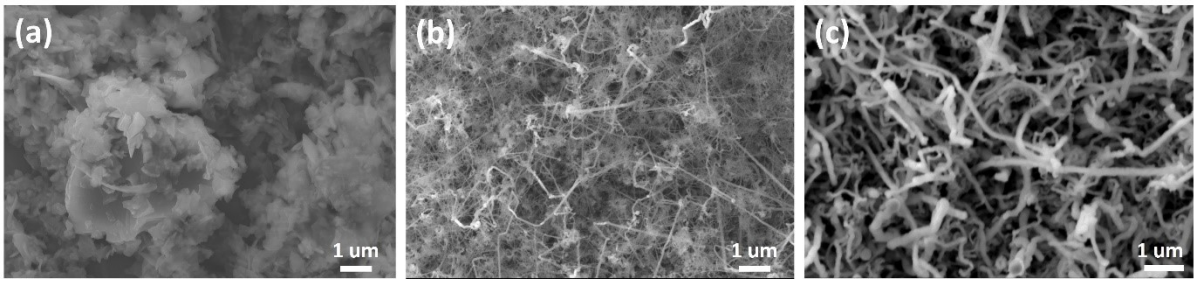

Fig. S11 SEM images of the (a) Si MPs, and the Si NWs that are grown on (b) stainless-steel fibre cloth (SSFC) and (c) planar stainless-steel sheet (SSS).

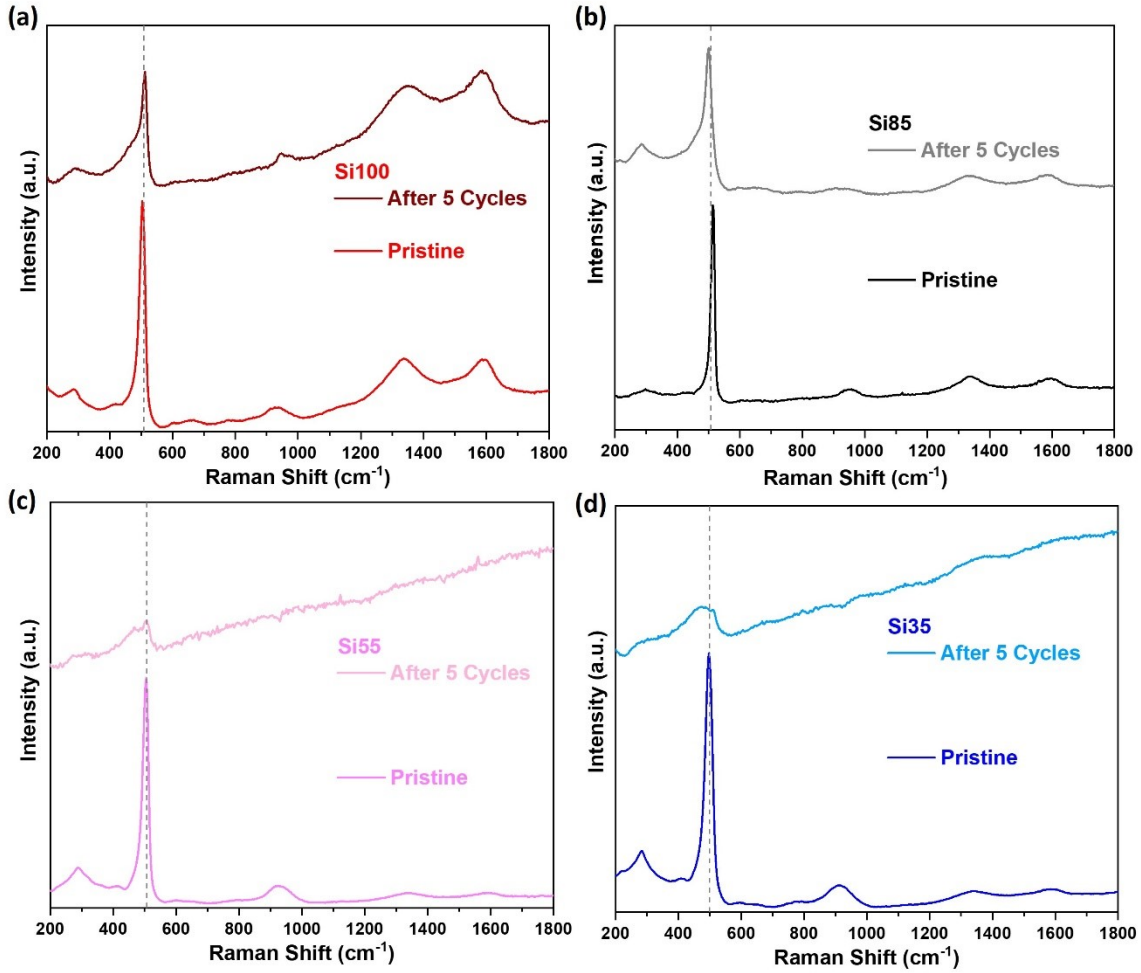

Fig. S12 Postmortem Raman spectrum analysis of (a) Si100, (b) Si85, (c) Si55, (d) Si35 after 5 cycles.

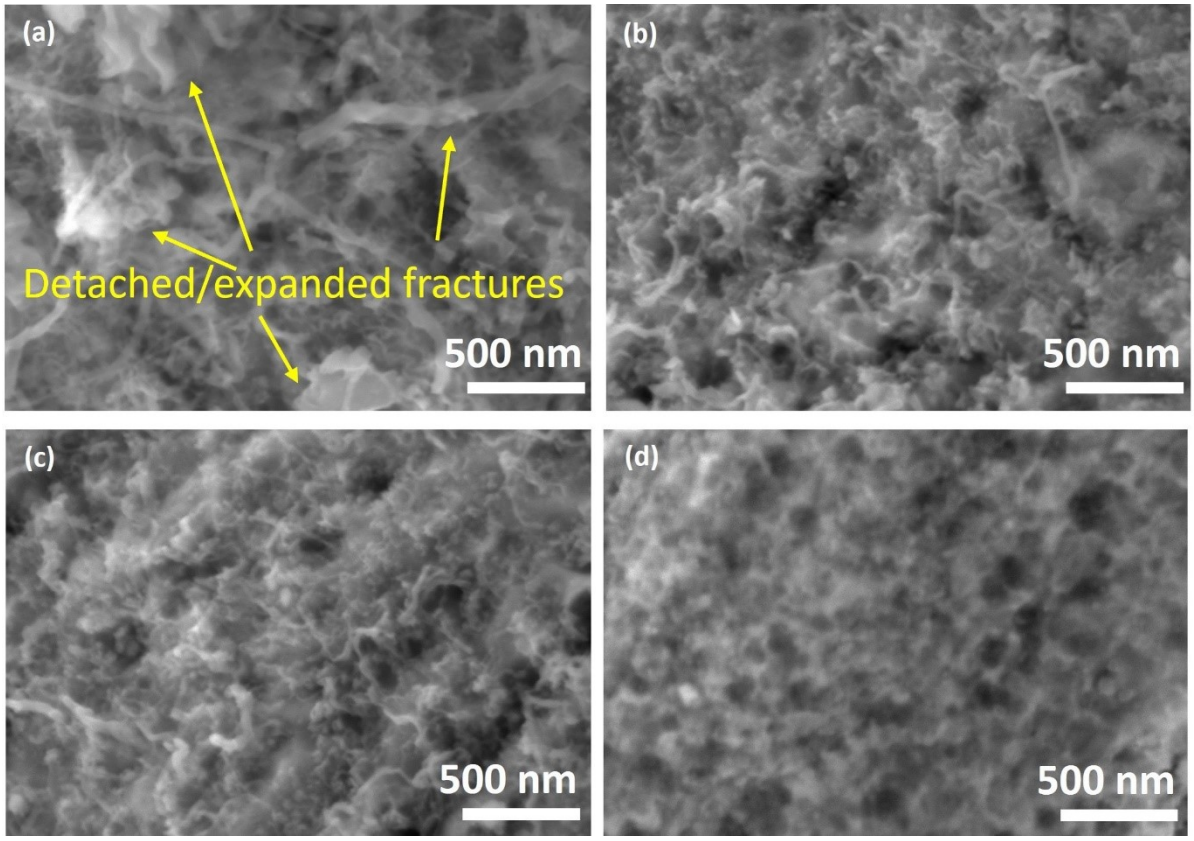

Fig. S13 Post-mortem SEM images of (a) Si100, (b) Si85, (c) Si55, (d) Si35 after 10 cycles.

Table S1. The values of FMHW and peaks area ratio of Si-Si in Raman spectra.

Sample	**Si100**	**Si85**	**Si55**	**Si35**
Peak Area ratio (%)	45.40	50.55	52.59	64.66
Raman – FMHW (cm^{-1})	19.4938	21.4090	23.5066	25.2622
FMHW (cm^{-1}) after 5 cycles	24.2818	25.9918	36.3657	N/A

Table S2. A comparison of the diameter of Si NWs, initial gravimetric capacities, initial Coulombic efficiency (ICE), and capacity retention for previously published Si-based anodes.

Material	Rate (mA/g)	Initial capacity (mAh/g)	ICE (%)	Capacity retention (%)	References
Si100	100	3554	62.1	63.5	This work
Si85	100	2218	76.4	80.0	This work
Si55	100	2409	74.3	82.3	This work
Si35	100	2602	75.4	87.3 (300 cycles)	This work
Si NWs @SSFC (72 nm)	350	2233	49.0	77.72% (100 cycles)	[1]
Si NWs without surface layer (30-250 nm)	1 mA/cm^2	4000	-	23.3 (400 cycles)	[3]
Si@ copper (400 nm)	80	1000	70	60% (60 cycles)	[4]
Si NWs@CF (250 nm)	0.1 mA/cm^2	3100	-	43.5 (200 cycles)	[5]
Ge-Si NWs (88 nm)	C/10	2090	65.8	82.9 (100 cycles)	[2]
Si NWs@C (160 nm)	C/10	2000	-	65 (100 cycles)	[6]
Si-SiO_x NWs (15-40 nm)	C/10	2633	69	95 (80 cycles)	[7]
Si NWs–CNT (35-55 nm)	200 (C/2)	2360	88.8	- (35 cycles)	[8]
c/a Si NWs (149 nm)	C/30	3500	-	31.4 (60 cycles)	[9]
Si NWs (36 nm)	C/20	1077	66	14% (75 cycles)	[10]
Si NWs@ Graphite (20 nm)	C/5	1747	72	80% (200 Cycles)	[11]

References

1 S. Imtiaz, I. S. Amiinu, D. Storan, N. Kapuria, H. Geaney, T. Kennedy and K. M. Ryan, *Adv. Mater.,* 2021, **33**, 2105917.

2 T. Kennedy, M. Bezuidenhout, K. Palaniappan, K. Stokes, M. Brandon and K. M. Ryan, *ACS Nano*, 2015, **9**, 7456–7465.

3 N. Harpak, G. Davidi, D. Schneier, S. Menkin, E. Mados, D. Golodnitsky, E. Peled and F. Patolsky, *Nano Lett.*, 2019, **19**, 1944–1954.

4 F. Dogan, L. D. Sanjeewa, S.-J. Hwu and J. T. Vaughey, *Solid State Ion*, 2016, **288**, 204–206.

5 E. Peled, F. Patolsky, D. Golodnitsky, K. Freedman, G. Davidi and D. Schneier, *Nano Lett.*, 2015, **15**, 3907–3916.

6 T. D. Bogart, D. Oka, X. Lu, M. Gu, C. Wang and B. A. Korgel, *ACS Nano*, 2014, **8**, 915–922.

7 K. W. Lim, J. I. Lee, J. Yang, Y. K. Kim, H. Y. Jeong, S. Park and H. S. Shin, *ACS Appl Mater Interfaces*, 2014, **6**, 6340–6345.

8 X. Li, J.-H. Cho, N. Li, Y. Zhang, D. Williams, S. A. Dayeh and S. T. Picraux, *Adv Energy Mater*, 2012, **2**, 87–93.

9 H. Chen, J. Xu, P. Chen, X. Fang, J. Qiu, Y. Fu and C. Zhou, *ACS Nano*, 2011, **5**, 8383–8390.

10 C. K. Chan, R. N. Patel, M. J. O'Connell, B. A. Korgel and Y. Cui, *ACS Nano*, 2010, **4**, 1443–1450.

11 S. Karuppiah, C. Keller, P. Kumar, P. H. Jouneau, D. Aldakov, J. B. Ducros, G. Lapertot, P. Chenevier and C. Haon, *ACS Nano*, 2020, **14**, 12006–12015.